Int. J. Electrochem. Sci., 12 **(2017)** 11972 – 11986, doi: 10.20964/2017.12.62

International Journal of
ELECTROCHEMICAL
SCIENCE
www.electrochemsci.org

Influence of the Deposition Temperature on the Electrodeposition Mechanism of Zn-Co-Fe Alloy

O. K. Al-Duaij[*]*, M. M. Abou-Krisha and M. I. Attia*

College of Science, Chemistry Department, Al Imam Mohammad Ibn Saud Islamic University
(IMSIU), Riyadh 11623, KSA
[*]E-mail: okduaij@imamu.edu.sa

Received: 1 August 2017 / *Accepted:* 18 October 2017 / *Published:* 12 November 2017

Steel was protected by coating its surface with a zinc-cobalt-iron alloy in a sulfate bath at different temperatures. Many techniques were used to analyse the composition, morphology and phase structure of the coating. A galvanostatic method was utilized to investigate the compositional and structural changes resulting from changes in the plating temperature. The results indicated that varying the deposition temperature led to anomalous and normal co-deposition of zinc, iron and cobalt. For temperatures higher than 50°C, a sharp decrease in the current efficiency of the zinc-cobalt-iron co-deposition was observed. The decrease in the current efficiency with the increase in the deposition temperature may be due to an increase in hydrogen evolution, which decreases the current efficiency of zinc. At 60°C, sharp transformations in the compositions and phase structures of the zinc-cobalt-iron alloy coatings were detected. The changes in the cathodic potential may have resulted in increased cobalt and iron contents in the zinc-cobalt-iron alloy coatings as the deposition temperature increased. The alloy showed a compact morphology and acceptable corrosion resistance when the temperature was in the 30-40°C range.

Keywords: Anomalous co-deposition, Zn-Co-Fe alloy, Electrochemical properties; Corrosion

1. INTRODUCTION

Zinc alloys have better anti-corrosion properties than zinc and are utilized as coatings for ferrous substrates in the automobile industry [1]. Zn alloys are a substitute for expensive and harmful cadmium coatings [2, 3]. Common zinc alloys include Zn-Co, Zn–Fe and Zn-Ni [1-4]. The co-deposition of Fe into a binary Zn-Co alloy or Co into a binary Zn–Fe alloy changes the appearance and performance of the produced ternary Zn-Co-Fe alloy. Currently, electrodeposited Zn-Co-Fe alloys have attracted attention because of their good protection properties [5-7]. The deposition mechanism for these alloys is not well understood because the co-deposition procedures are complex. In the electrochemical approach, the equilibrium potentials of iron and cobalt are more positive than those of zinc, and their deposition should be more favourable than that of zinc. However, zinc is favourably deposited in most processes [8–11]. A few hypotheses have been suggested to clarify this phenomenon, and the purported 'hydroxide suppression mechanism' (HSM) is commonly accepted [12]. According to this hypothesis, the preferential deposition of zinc may be ascribed to hydrogen evolution during the zinc–iron metal alloy deposition. Hydrogen evolution can increase the pH on the cathode surface and result in the formation of $Zn(OH)_2$, on the electrode surface, which can act as a selective membrane film and hinder the association of iron metal ions with the electrolyte on the cathodic surface. Considering this mechanism, the deposition parameters that result in increasing the pH of the zinc–iron metal electrolyte may promote zinc deposition. In contrast to the HSM theory, Chassaing and Fabri Miranda [13, 14] observed that the zinc content in coatings decreased with an increase in the pH of the zinc–iron metal alloy electrolyte. An alternate principle proposes that since the zinc deposition potential on the surfaces of iron metals will be higher than that on the surfaces of different metals, the preferential deposition of zinc may be due to the deposition of zinc on the surface of iron metals [15–17]. Under some specific conditions, e.g., a low current density and low plating potential, this hypothesis cannot explain why zinc continues to deposit after fully coating the surface or the preferential deposition of iron metals [18–21]. In alloy plating, the co-deposition procedure is influenced by a number of factors, e.g., the bath deposition potential, structure, current density, temperature and bath pH [18, 23–31]. If the zinc–iron aggregate metal co-deposition mechanism is determined for various plating conditions, a commendable standard may be created. Since the temperature influences the deposition rate, composition, structure, and properties of alloys, it is a significant factor and has the most influence on the electrodeposition of alloys [19, 32]. The diffusion of a metal ion from the electrolyte to the cathode typically improves as the temperature increases, and the deposition rate may be related to the deposition temperature [33–36]. The impact of the temperature on the electrodeposition of zinc–nickel alloy from different baths needs to be studied [19, 36]. The nickel amount in zinc–nickel alloy coatings might be related to the deposition temperature, and this can be determined by fixing the different plating parameters. However, the principle goal for these types of investigation has been to streamline electroplating processes, and the structure and composition changes prompted by temperature variations have not been studied.

In the current work, the effects of the plating temperature on the coating and electrodeposition qualities of a zinc–cobalt-iron alloy from a sulfate bath were studied. Scanning electron microscopy (SEM), X-ray diffraction (XRD) and energy dispersive spectroscopy (EDS) were used to portray the structures, morphologies, and compositions of the coatings. Galvanostatic and potentiostatic techniques were used to inspect the composition and structure changes incited by variations in the deposition temperature.

2. EXPERIMENTAL

The electrolyte used in the electrodeposition consists of 0.2 M $ZnSO_4$, 0.2 M $CoSO_4$, 0.2 M $FeSO_4$, 0.2 M Na_2SO_4, 0.2 M H_3BO_3 and 0.01 M H_2SO_4. All reagents were analytical grade, and the electrolytes were prepared using doubly distilled water. To guarantee the accuracy of the analyses and results, the experiments were performed in duplicate. The electrolytic cell was utilized as shown in Ref. [36]. The cell was washed with distilled and doubly distilled water after it was cleaned with a sulfuric/chromic acid mixture. The cell contained 50 cm^3 of the electrodepositing solution at the selected deposition temperature, and an air thermostat was used to guarantee control of the temperature. A Pt electrode was used as a counter electrode, and a standard calomel electrode (SCE) was used as the standard electrode. A steel rod was used as the cathode for the deposition. The cathode was placed in a Teflon mount to allow a cross-sectional region of 0.196 cm^2 to be in contact with the solution. The electrodes were maintained using the procedures described in Ref. [37].

Cyclic voltammetry (CV), potentiostatic current density-time (PCDT) and *g*alvanostatic method (GM) tests were performed on the steel rod. All CV experiments started with a negative sweep at 0.0 V to -1.3 V and then returned at a scan rate of 5 mV s^{-1}. Anodic linear sweep voltammetry (ALSV), potentiodynamic polarization resistance (PPR) analysis and chemical composition analysis were performed immediately after the galvanostatic deposition. The Zn-Co-Fe alloys were stripped using potentiodynamic circumstances: (i) an electrolyte similar to that used in the electrodeposition for cyclic estimations, (ii) 0.5 M Na_2SO_4 + 0.05 M EDTA electrolyte for anodic linear sweep voltammetry (ALSV), and (iii) 0.05 M HCl electrolyte for the (PPR) stimations. Electrochemical measurements were performed using an EG&G potentiostat/galvanostat model 273A, which was controlled by a personal computer using the 352 corrosion analysis software.

The surface morphology, chemical contents and phase compositions were determined using an SEM instrument (model JSM-5500 LV, JEOL), an EDS (energy dispersive X-ray spectroscopy) system connected using Isis® programming, a model 6587 X-ray detector (Oxford, UK) and BRUKER Axs-D8 Advance model XRD instrument with CuKα radiation (λ = 1.5406 Å, 40 mA). For the determination of the morphological properties (SEM) and contents of the electrodeposited alloy, 1.0 cm width and length samples of the steel and stainless-steel sheet cathodes were utilized. The alloy was electrodeposited on a copper sheet for EDS and XRD characterization to prevent the challenges caused by the deposits containing Fe. An AAS model AA–6701F (SHIMADZU) instrument was used to determine the chemical composition of each deposit. The deposits were dissolved in 50 cm^3 30% (V/V) hydrochloric acid, and diluted with doubly distilled water up to 100 cm^3. The cathode current efficiencies and the film thicknesses [37] of the deposits on the SS substrate were determined. The electrochemical corrosion estimations for the plated deposits, the corrosion potential ($E_{corr.}$), the polarization resistance (R_p) and the corrosion current ($I_{corr.}$) were obtained [38].

3. RESULTS AND DISCUSSION

3.1. Cyclic voltammograms

The temperature was found to have a noticeable effect on the appearance and composition of the deposit. The cyclic voltammograms for the Zn-Co-Fe alloys obtained on a steel rod substrate at different depositing bath temperatures are illustrated in Figure (1). In the cathodic scan, a cathodic peak current (C_1) appears at approximately -750 mV and is probably due to the deposition of sulfur, which occurs due to the presence of H_2SO_4 [39]. This peak increases with the increasing temperature. The same result was observed for another alloy in a published paper [38]. However, M. H. Seo et al. demonstrated that the sulfur content in deposits from a Ni sulfamate bath, which is unlike the current bath, decreased as the temperature of the electrolyte increased to 60°C, and this is contrary to the current results [26]. At low temperatures, 10°C and 20°C, another cathodic peak (C_2) appears before the HER occurs, and the peak can be ascribed to late deposition of the alloy components before the HER decreases at these temperatures.

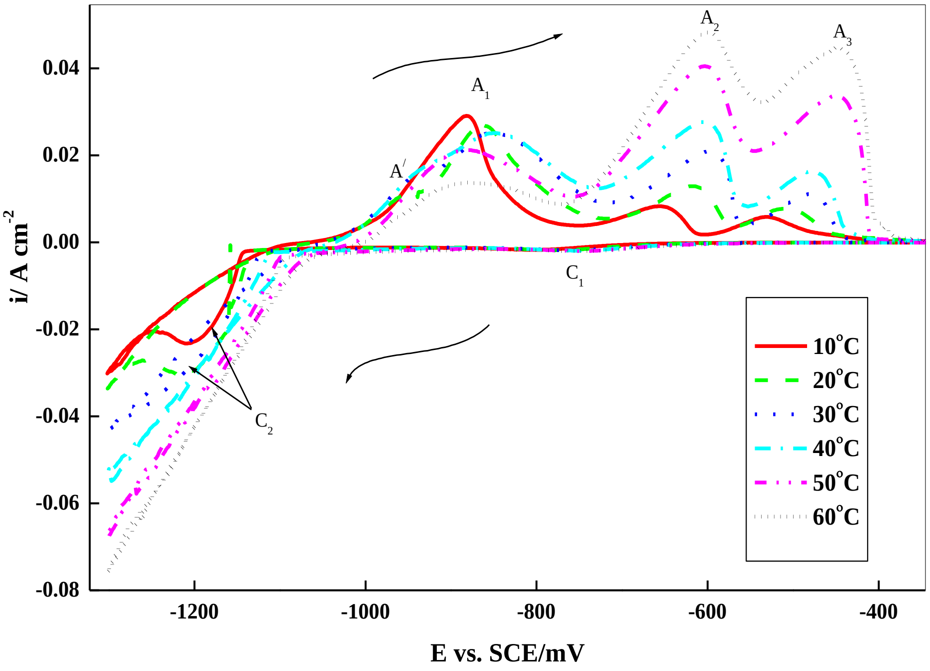

Figure 1. i-E curves (CVs) for steel in a standard bath at 10°C, 20°C, 30°C, 40°C, 50°C and 60°C and a scan rate of 5 mV s^{-1}.

(a)

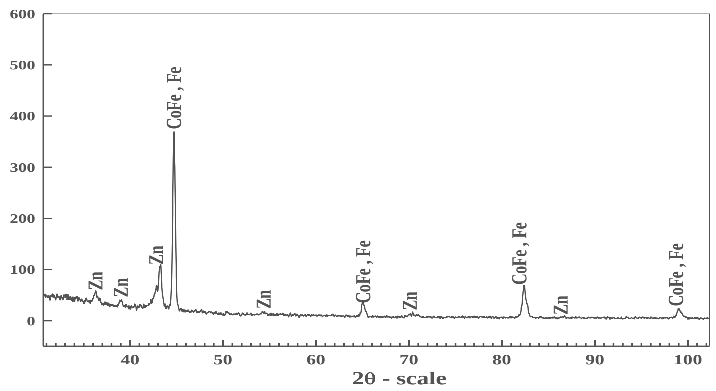

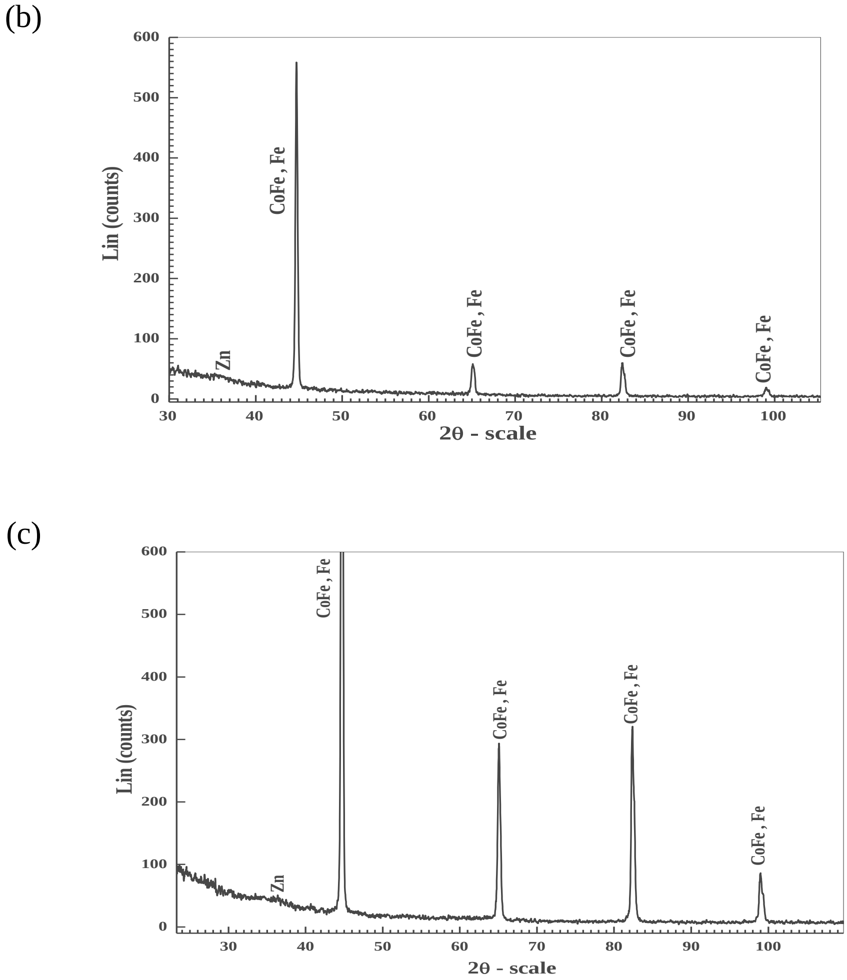

Figure 2a-c. XRD patterns for Zn-Co-Fe alloy electrodeposited on a copper substrate at 10 mA cm^{-2} from a standard bath at different temperatures for 10 min (a- 20°C, b- 40°C and c- 60°C).

Additionally, by increasing the plating temperature, the cathodic deposition current peak increases because of the parallel increase in the cathodic charge, which lessens the nucleation overpotential. N. D. Nikolić et al. considered the impact of the temperature on the electrodeposition of disperse copper deposits and showed that increasing electrodeposition currents may be observed with an increasing temperature [40]. Increases in the current density as the temperature increases, are expected because a higher temperature reduces the viscosity of the solution and creates less resistance against ion movement and current formation. The increase in the current density, enhanced the amount electrodeposited and consequently increased the thickness of the alloy deposit [41]. The deposition potentials shifted to higher anodic potentials as the bath temperature increased from 10°C to 60°C; this could be attributed to the effect of the temperature on the dischargeable ion diffusion rates and activation overpotentials [34]. Therefore, the Co and Fe contents in the film increase as the plating temperature increases. For the zinc content in the plating film, the situation is reversed, as shown in Table (1). Therefore, higher bath temperatures are more beneficial for cobalt and iron deposition and not zinc. Increasing the plating temperature should accelerate the mass transport of the metal ions to the cathode and help overcome the energy barrier for metal deposition. The XRD results in Figure (2 a-c) demonstrate the impact of the bath temperature on the phase structure. Increasing the temperature leads to a change in the peak height of the formed phases. Under the inspected conditions, the deposits contain pure zinc and pure iron/FeCo phases. The pure Zn peak height decreases, and the pure iron/FeCo phase peak heights increase with the increasing temperature.

Table (1): Zn, Co and Fe quantities in the deposit;, the total weight of the deposit;, the percentages of Zn, Co and Fe; the, current efficiencies of Zn, Co, Fe, and Zn-Co-Fe deposits; the, thickness;, and electrochemical corrosion measurements of the deposit, galvanostatically deposited from a standard bath at 10 mA cm^{-2} for 10 min, at 20°C, 30°C, 40°C, 50°C and 60°C.

Temperature / °C Parameter	20	30	40	50	60
Zn amount in the deposit / 10^{-5} g	175	165	157	130	120
Co amount in the deposit / 10^{-5} g	8.3	9.2	11.6	13.8	18.6
Fe amount in the deposit / 10^{-5} g	15.3	17.9	18.5	19.4	19.5
Total mass of the deposit / 10^{-5} g	199	192	187	163	158
Zn content / %	88.1	85.9	83.9	79.8	75.9
Co content / %	4.2	4.8	6.2	8.3	11.8
Fe content / %	7.7	9.3	9.9	11.9	12.3
Zn Current efficiency (e_{Zn}) / %	86.1	81.2	77.3	64.0	59.0
Co Current efficiency (e_{Co}) / %	4.5	5.0	6.3	7.5	10.2
Fe Current efficiency (e_{Fe}) / %	8.8	10.3	10.7	11.17	11.23
Zn-Co-Fe deposit current efficiency ($e_{Zn\text{-}Co\text{-}Fe}$) / %	99.4	96.5	94.2	82.6	80.4
Thickness of the deposit / µm	1.37	1.32	1.28	1.11	1.06
R_p / K-Ohms	0.8	0.87	0.94	0.99	1.4
$I_{corr.}$ / mA cm^{-2}	1.33	1.27	1.18	1.11	0.7
($E_{corr.}$) Corrosion potential / mV	-945	-943	-931	-925	-808

Figure (1) shows the three anodic dissolution peaks and the appearance of a shoulder as the temperature increases for the anodic scan. The shoulder and first anodic peak correspond to the dissolution of zinc from pure zinc, and the heights diminish as the bath temperature increases, which implies the zinc deposition rate decreases (pure zinc phase). The second anodic peak is due to the dissolution of Fe from pure iron and from the FeCo phase, and the third peak corresponds to the dissolution of Co from the FeCo phase. The second and third anodic peaks increase as the plating bath temperature increases. The anodic dissolution peaks shift to more positive potentials as the bath temperature increases from 10°C to 60°C, resulting in an enhancement in the alloy corrosion resistance.

The decrease in both the cathodic efficiency and Zn content in the alloy deposition as the temperature increases can be attributed to hydrogen evolution on the cathode surface instead of the deposition of the metallic coating. Thus, increasing the temperature of the plating bath, a couple of degrees, can moderate the nature of the co-deposition and decrease the zinc content in the deposit [35]. The HSM mechanism states that the nickel deposition can be hindered by $Zn(OH)_2$. Consequently, the nickel content and partial current should decline as the deposition temperature increases. The experimental results do not agree with the results expected based on the HSM mechanism [35]. The increase in the cobalt and iron content can be credited to a reduction in the overpotential of cobalt and iron at higher temperatures. The cyclic voltammetric curves clearly show that increasing the temperature, from 10°C to 60°C, results in a decrease in the zinc deposition rate, as indicated by the decrease in the first anodic peak. However, the second and third peaks shift in the positive direction as a result of the increased iron and cobalt contents.

3.2. Galvanostatic measurements and anodic linear sweep voltammograms

The galvanostatic curves for the Zn-Co-Fe alloy deposited on a steel rod substrate at 10 mA cm^{-2} for 10 minutes at different deposition temperatures are given in Figure (3). The deposition potential depends on the plating bath temperature. A fast decrease in the deposition potential followed by a steady value during the first few seconds indicates the end of the growth of the deposited film. The deposition potentials incrementally shift to more positive values as the temperature of the bath increases.

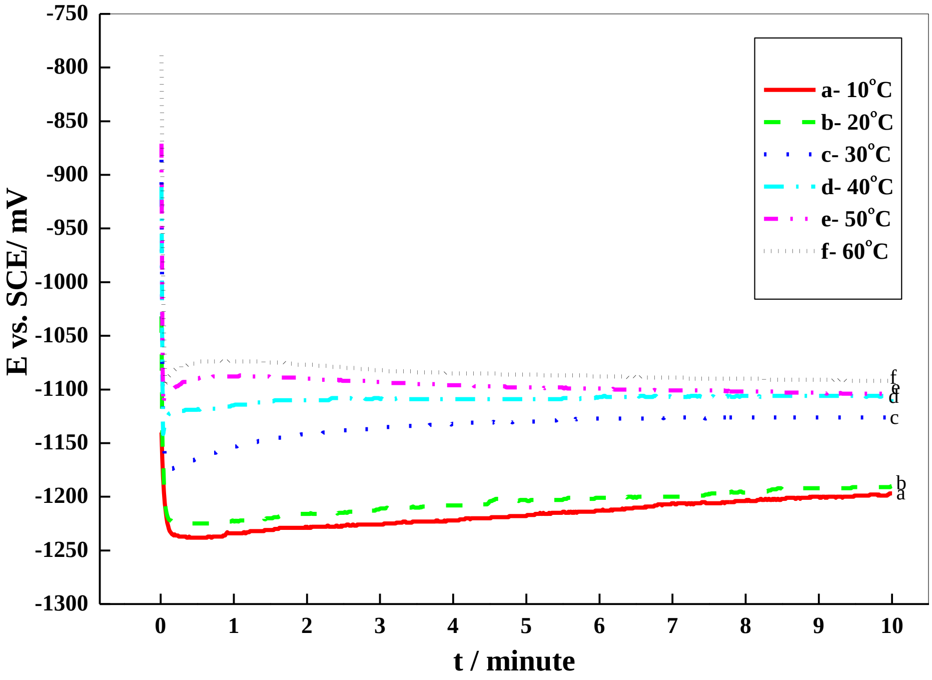

Figure 3. E-t curves for steel in a standard bath at different temperatures for 10 min at 10 mA cm^{-2} (a- 10°C, b- 20°C, c- 30°C, d- 40°C, e- 50°C and f- 60°C).

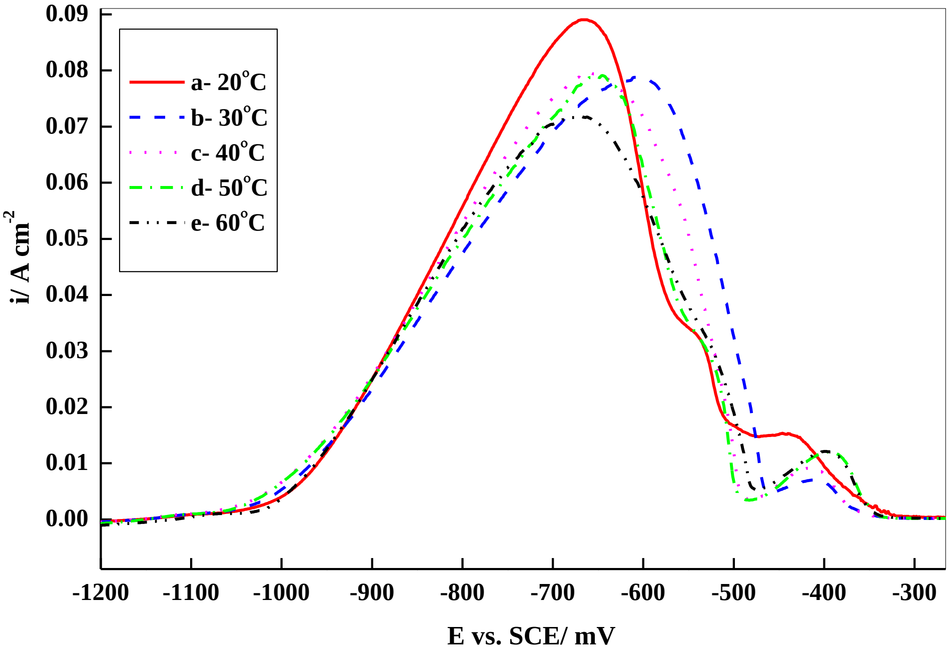

Figure 4. ALSVs for a Zn-Co-Fe alloy, galvanostatically electrodeposited on steel rod from a standard bath at 10 mA cm^{-2} for 10 min, at different temperatures (a- 20°C, b- 30°C, c- 40°C, d- 50°C and e- 60°C), in a Na_2SO_4+EDTA solution at a scan rate of 5 mV s^{-1}and 25°C.

As indicated by Figure (3), a lower overpotential is required to create a premier nucleus during deposition from a bath with a higher temperature, but at lower temperatures, additional overpotential is required. The contents of both the cobalt and iron components increase as the bath temperature increases, as shown in Table (1), and this increases the corrosion resistance of the alloy. This result can be explained by the increasing diffusion coefficients and intensity of the metal in the electrical double layer. A comparable outcome was observed for Zn-Ni-Fe alloy deposition in a published paper [39].

Figure (4) shows the ALSVs for the Zn-Co-Fe alloys that were galvanostatically deposited on a steel rod substrate for 10 min at different temperatures and then dissolved in a Na_2SO_4+EDTA solution. When an alloy film is anodically polarized under potentiodynamic conditions, the contents will dissolve at different potentials, based on their kinetic properties and equilibrium. The different phase structures and chemical forms that exist in the alloy will generate different current peaks. Thus, the peak obtained is characteristic of the alloy constituents and the phase structure of the film [42-43]. The fundamental issue with the utilization of this technique is discovering a convenient electrolyte in which the electrodeposited material will dissolve slowly and completely. Zinc alloys ’do not dissolve in Na_2SO_4 solutions, but in the presence of (EDTA,) Zn and its alloys dissolve [42-43]. The dissolution of the Zn-Co-Fe alloy resulted in three anodic dissolution peaks at potentials of -667 mV, -525 mV and -400 mV. These three current density peaks represent the dissolution of zinc from the pure zinc phase, and the second anodic peak represents the dissolution of Fe from the pure Fe and FeCo phases. The third anodic peak is ascribed to the dissolution of Co from the FeCo phase. In the same figure at 20°C, the height of the first zinc dissolution peak indicates the large amount of zinc. Increasing the temperature of the deposition bath generally leads to a decrease in the height of the first anodic peak and increases in the heights of the second and third anodic peaks.

3.3. Potentiostatic current density-time curves

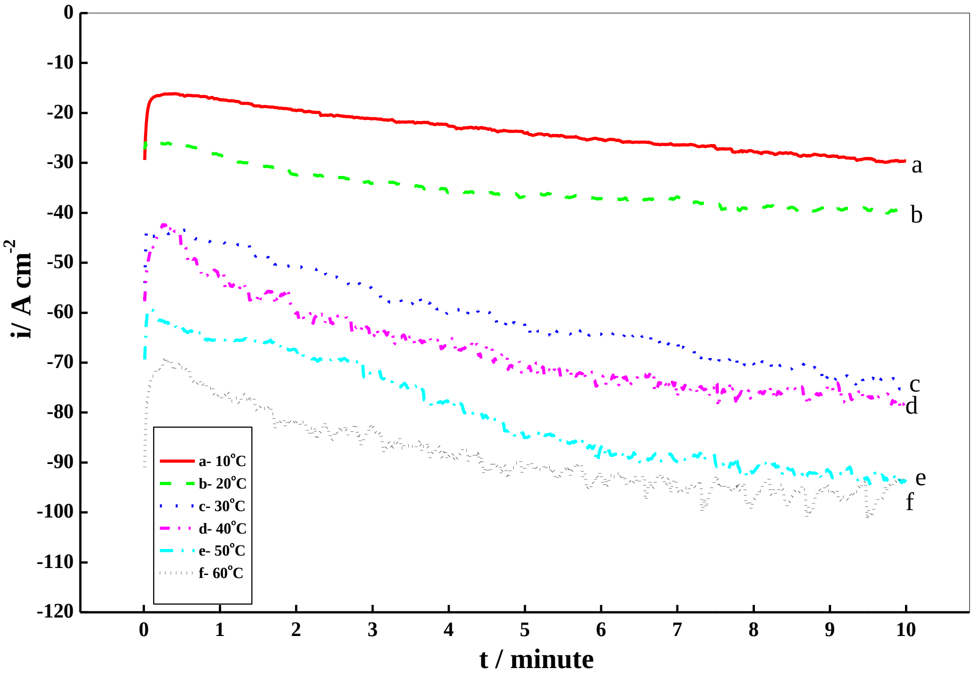

Figure 5. i-t curves for steel in a standard bath at different temperatures (a- 10°C, b- 20°C, c- 30°C, d- 40°C, e- 50°C and f- 60°C) for 10 min at -1300 mV.

Figure (5) shows the potentiostatic deposition curves for the Zn-Co-Fe alloy deposited on steel for 10 min at -1300 mV. According to Figure (5), increasing the temperature increases the cathodic current in the cathodic direction, which may cause an increase in the deposition rate of the metals [44].

At 10 and 20°C, the initial current density of -16.8 and -25.9 mA cm^{-2}, respectively, increases to a maximum in the first 15 s and then slightly decreases, which may be due to the deposit plating out on the electrode surface. From 30 to 60°C, the nucleation process occurs in approximately 15 s and an obvious decrease in the current occurs, resulting in extra deposition of ()Co and Fe and the deposit covering the electrode surface. The development of these covering appears to be related to the deposition of Co and Fe on the Zn coating surface. Variations may be a consequence of hydrogen evolution via H_2 bubbles.

3.4. Potentiodynamic polarization curves

Figure (6) displays the corrosion resistance properties of the Zn-Co-Fe alloy potentiostatically deposited at different temperatures for 10 minutes and dissolved in a 0.05 M HCl solution. The values of the corrosion potentials ($E_{corr.}$) were estimated from this figure and are shown in Table (1). The corrosion potentials ($E_{corr.}$) indicate the deposit dissolution resistance in a corrosion medium. The figure shows that the E_{corr} values at higher temperatures shift increase compared with those obtained at lower temperatures, and this may be due to the increased contents of cobalt and iron at higher temperatures.

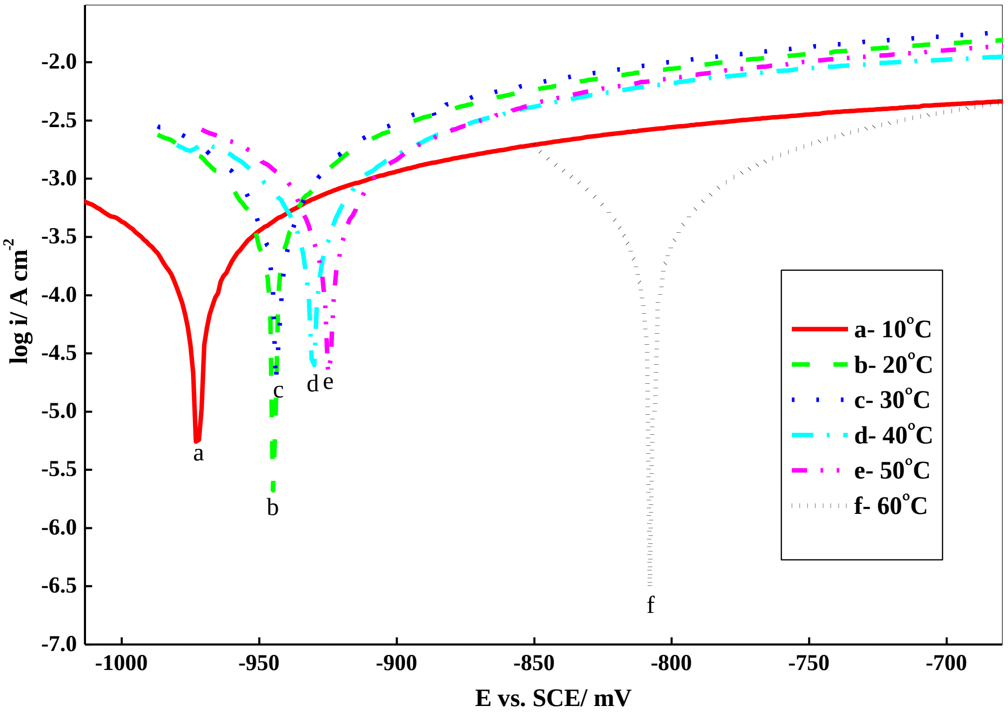

Figure 6. log i- E for the Zn-Co-Fe alloy, galvanostatically electrodeposited on a steel rod substrate from a standard bath at different temperatures (a- 10°C, b- 20°C, c- 30°C, d- 40°C, e- 50°C and f- 60°C) for 10 min at -1300 mV, in a 0.05 M HCl solution at a scan rate of 5 mV s^{-1} and 25°C.

3.5. Surface morphology

To understand the corrosion protection mechanism, the morphology of the deposits must be understood. The surface morphology of the deposited film mainly depends on the temperature of the electrolyte bath. Increasing the plating bath temperature should accelerate the mass transport of metal ions to the cathode and help overcome the energy barrier for metal deposition [45]. In this case, the effect is more pronounced for cobalt and iron. Increasing the plating bath temperature can also help reduce the stress and cracking in the deposit films (Figure 7a-c). The deposit obtained at the lowest temperature, 20°C, has an inhomogeneous structure, as shown in Figure 7a.

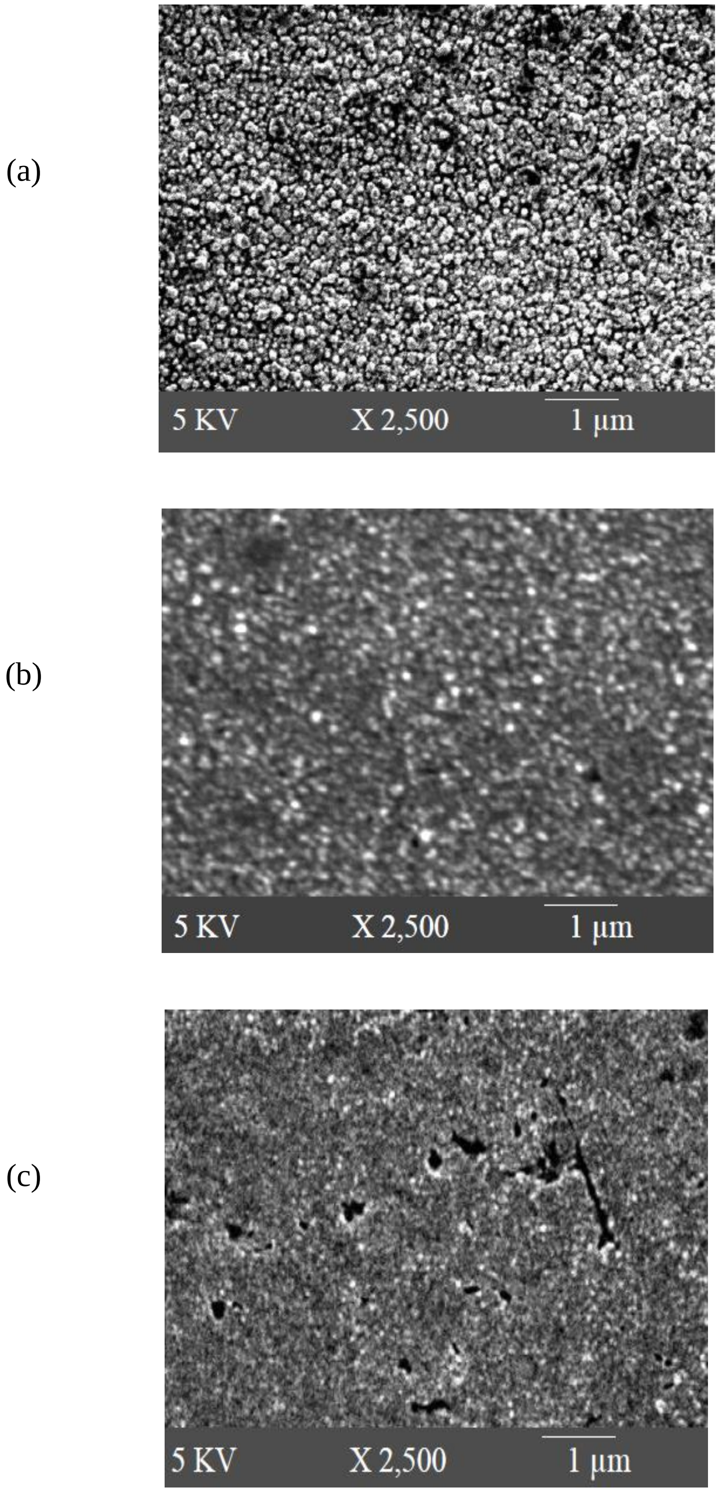

Figure (7a-c). SEM photographs of the Zn-Co-Fe alloys electrodeposited on a steel sheet substrate from a standard bath at a- 20°C, b- 40°C and c- 60°C for 10 min at 10 mA cm^{-2}.

The inhomogeneous morphology of the obtained alloy deposits may be due to the high content of Zn. As the temperature increases to 40°C, compact, fine-grained particles begin to develop on the surface (Figure 7b). Therefore, a further increase in the temperature reveals a compact and uniform layer of alloy particles over the whole surface. Additionally, as the temperature increases, Fe and Co are more easily deposited and quickly replenished at the cathode, which demonstrates that the deposition procedure is diffusion controlled. N. D. Nikolić et al. [40] elucidated that the decrease in the grain size with the increasing temperature might be due to the well-known dependence of the nucleation rate on temperature [46].

Upon additional increases in the deposition temperature (Figure 7c), the compactness of the covering begins to degrade, and, a few voids and cracks can be observed on its surface [35, 47]. The manifestation of the cracks in the coating can possibly be attributed to the hydrogen evolution [34]. Upon the reduction of hydrogen, a few hydrogen atoms absorb on the surface of the covering and diffuse inside the coating;, subsequently, the crystal lattice of the covering can be strained by the hydrogen atoms trapped in the coating, and a high residual stress appears [21].

The grain size of the deposited alloys was calculated using Sherres's equation (1)

$$D = (K\lambda) / (\beta \cos \theta) \qquad (1)$$

where K is 1, λ is the wavelength of the X-ray used, and β is the full width of the half maximum of the peak. The calculated grain sizes at 20, 40 and 60°C, for the Zn-Co-Fe film are small and in the nanosize range, 65.6, 25.7 and 17.3 nm, respectively.

3.6. The chemical composition of the deposit alloys and electrochemical measurements

The effect of the temperature on the percentages of Co, Fe and Zn in the Zn-Co-Fe alloy from the sulfate bath is shown in Table (1). At low temperatures, the zinc content in the alloy is relatively high, due to the anomalous co-deposition. Otherwise, the increasing temperature tends to increase the content of cobalt and iron. The increases in the cobalt and iron contents in the alloy films at higher temperatures are attributed to an increase in the Co and Fe deposition kinetics and the minor overpotential for Co and Fe deposition. Additionally, increasing the plating bath temperature increases the rate of diffusion and convection, resulting in an increase in the concentration of metal ions in the cathodic diffusion region. Below these conditions, the cobalt and iron were deposited instead of zinc. This outcome reveals the greater effectiveness of diffusion over depolarization. The results obtained were in agreement with an earlier report [39] on the electrodeposition of Zn-Ni-Fe alloys in an acidic bath.

Table (1) shows the temperature dependence of the cathodic current efficiency for the Zn-Co-Fe alloy deposition. The cathodic current efficiency decreases with the increasing temperature; this can be ascribed to the (HER). Furthermore, the effect of the temperature on the thickness of the deposited film appears in the same table. The thickness of the deposited film decreases as the temperature increases, and this result can be attributed to a decrease in the zinc content of the alloy because zinc has a low density.

The positive corrosion potential increased as the plating temperature increased from -945 mV at 20°C to -808 mV at 60°C, and a decrease in the corrosion current density from 1.33 mA/cm^2 at 20°C to 0.7 mA/cm^2 at 60°C was achieved. The polarization resistance increased from 0.8 kΩ for the Zn-Ni alloy to 1.4 kΩ as the plating bath temperature increased from 20°C to 60°C. Based on these results, the alloy coating deposited at higher temperatures has better corrosion resistance properties than those of the alloy coating deposited at lower temperatures.

Those results imply a trend for the alloy deposition: Co^{2+} (or its monovalent intermediate Co^{+1}) will be adsorbed, followed by the adsorption of Fe^{2+} and then Zn^{2+} (or their monovalent intermediates, Fe^{+1} and Zn^{+1}) onto the newly adsorbed and deposited cobalt. The adsorption of zinc ions inhibits the deposition from claiming Co and Fe, but the adsorption does not completely block this.

This behaviour might be explained by the expanding diffusion coefficients and metal concentration in the electrical double layer due to the increase in the temperature. A higher temperature creates an expanded ion source for the cathode, a diminished activation energy for the nucleation, and a diminished electrolyte viscosity. The expanded dissociation of the metal complex was a thermodynamic result of the high temperature [48]. Therefore, the polarization for the electrodeposition should decrease as the temperature of the electrolyte increases. The increased electrolyte temperature diminished the Zn content in the deposits and decreased the polarization, which demonstrated that the deposition mechanism could be a normal deposition. Normal deposition behaviour predicts that a decrease in the polarization will decrease the content of the less noble metals in the deposits.

4. CONCLUSION

- By altering the deposition temperature under galvanostatic circumstances, the anomalous and normal co-depositions of Zn, Co and Fe were observed.
- The cobalt and iron contents in the Zn-Co-Fe coatings and the cathode potential abruptly increased once the deposition temperature reached 60°C.
- When the plating temperature was higher than 30°C, the current efficiency of the deposition clearly decreased.
- An increase in hydrogen evolution resulted in a decrease in the current efficiency of the Zn-Co-Fe deposition with the increase in deposition temperature.
- The most suitable plating temperature was between 30–40°C because the obtained Zn-Co-Fe alloy covering had a compact morphology and no cracks.

ACKNOWLEDGEMENT
The researchers thank the Deanship of Scientific Research at Al Imam Mohammad Ibn Saud Islamic University, (IMSIU), Riyadh, KSA for funding this project, No. 341208/1434 H.

References

1. T. Tsuru, S. Kobayashi, T. Akiyama, H. Fukushima, S.K. Gogia and R. Kammel, *J Appl Electrochem*, 27 (1997) 209.
2. C.R. Tomachuk, C.M.A Freire, M. Ballester, R. Fratesi and G. Roventi, *Surf. Coat. Tech.*, 122 (1999) 6.

3. M.M. Abou-krisha and A.M. Abushoffa, *Int J Electrochem Sci*, 5 (2007) 418.
4. F. Azizi and A. Kahoul, *Transactions of the IMF,* 94 (2016) 43.
5. M. Ebadi, W.J. Basirun, Y. Alias, M.R. Mahmoudian and S Y Leng, *Mater Charact*, 66 (2012) 46.
6. Z.F. Lodhi, M.C. Mol, A. Hovestad, H.A. Terryn and J.H.W. De wit, *Surf. Coat. Tech*., 202 (2007) 84.
7. A.M.D. Conceicao, N.C. Eduardo and Z.N. Roberto, *J Mat Sci and Appl*, 3 (2012) 348.
8. J.B. Bajat, S. Stankovic, B.M. Jokic, *Surf. Coat. Tech*., 204 (2010) 2745.
9. H. Faid, L. Mentar, M.R. Khelladi and A. Azizi, *Surface Engineering,* 33 (2017) 529.
10. C. Srivastava, S.K. Ghosh, S. Rajak, A.K. Sahu, R. Tewari, V. Kain and G.K. Dey, *Surf. Coat. Tech*., 313 (2017) 8.
11. N. Eliaz, K. Venkatakrishna and A. Chitharanjan Hegde, *Surf. Coat. Tech*., 205 (2010) 1969.
12. A. Brenner, Electrodeposition of Alloys, Academic Press, New York, (1963).
13. F. Zhongbao, A. Maozhong, R. Lili, Z. Jinqiu, Y. Peixia and C. Zhiqiang, *RSC Adv.*, 6 (2016) 64726.
14. N. Loukil and M. Feki, *Appl. Surf. Sci.*, 410 (2017) 574.
15. M.J. Nicol and H.I. Philip, *J. Electroanal. Chem.*, 70, (1976) 233.
16. R.P. Oliveira, D.C. Bertagnolli, L. da Silva, E.A. Ferreira, A.S. Paula and G.S. da Fonseca, *Appl. Surf. Sci.*, 420 (2017) 53.
17. S. Swathirajan, *J. Electroanal. Chem.,* 221 (1987) 211.
18. F. Elkhatabi, M. Benballa and M. Sarret, *Electrochim Acta*, 44 (1999) 1645.
19. H.Y. Lee and S.G. Kim, *Surf. Coat. Tech*., 135 (2000) 69.
20. G. Roventi, R. Fratesi and R.A. Della Guardia, *J Appl Electrochem*, 30 (2000) 173.
21. R. Fratesi, G. Roventi, *J Appl Electrochem*, 22, 657 (1992).
22. G. Barcelo, J. Garcia and M. Sarret, *J Appl Electrochem,* 24 (1994) 1249.
23. R. Albalat, E. Gomez and C. Muller, *J Appl Electrochem*, 21 (1991) 44.
24. M.M. Abou-Krisha, *Mater. Chem. Phys.*, 125 (2011) 621.
25. S.M.S.I. Dulal, H.J. Yun and C.B. Shin, *Electrochim Acta*, 53 (2007) 934.
26. M.H. Seo, D.J. Kim and J.S. Kim, *Thin Solid Films,* 489 (2005) 122.
27. K.S. Lewa, M. Rajab and S. Thanikaikarasanb, *Mater. Chem. Phys.*, 112 (2008) 249.
28. M.A. Farzaneh, K. Raeissi and M.A. Golozar, *J Alloy Compd*, 489 (2010) 488.
29. C.K. Chung and W.T. Chang, *Thin Solid Films,* 517 (2009) 4800.
30. S.L. Diaz, O.R. Mattos and O.E. Barcia, *Electrochim Acta*, 47 (2002) 4091.
31. R. Oriˇnakova, A. Oriˇnak and G. Vering, *Thin Solid Films*, 516 (2008) 3045.
32. S.N. Srimathi and S.M. Mayanna, *Metal Finishing*, 11 (1985) 35.
33. L.C. Li, Y. Zhang and S. Deng, *Materials Letters*, 57 (2003) 3444.
34. S.S. Abdelrehim, E.E. Fouad and S.M. Abdelwahab, *Electrochim Acta*, 41 (1996) 1413.
35. X. Qiao, H. Li, W. Zhao and D. Li, *Electrochim. Acta*, 89 (2013) 771.
36. M.M.Abou-Krisha, *Appl. Surf. Sci.*, 252 (2005) 1035.
37. F. El-Chiekh, M.T. El-Haty, H. Minoura and A.A. Montaser, *Electrochim Acta*, 50 (2005) 2857.
38. M.M. Abou-Krisha, F.H. Assaf and S.A. El-Naby, *J. Solid State Electrochem.*, 13 (2009) 87.
39. M.M. Abou-Krisha, H.M. Rageh and E. Matter, *Surf. Coat. Tech.*, 202, (2008) 3739.
40. N. D. Nikolić, L. J. Pavlović, M. G. Pavlović and K. I. Popov, *J. Serb. Chem. Soc*., 72 (2007) 1369.
41. O. Sadiku-Agboola, E.R. Sadiku, O.I. Ojo, O.L. Akanji and O.F. Biotidara, *Portugaliae Electrochimica Acta*, 29 (2011) 91.
42. J.B. Bajat, M.D. Maksimovic and G.R. Radovic, *J. Serb. Chem. Soc.*, 67 (2002) 625.
43. J.B. Bajat, Z. Kacarevic-Popovic, V.B. Miskovic-Stankovic and M.D. Maksimovic, *Prog. Org. Coat.*, 39 (2000) 127.
44. F. H. Assaf, A. M. A. El-Seidy, M. M. Abou-Krisha and A. A. Eissa, *Int. J. Electrochem. Sci.*, 10 (2015) 5465.
45. G. Zangari, Coatings, 5 (2015) 195; doi:10.3390/coatings5020195.

46. E. Budevski, G. Staikov and W. J. Lorenz, Electrochemical Phase Formation and Growth, An Introduction to the Initial Stages of Metal Deposition, VCH Weinheim, New York, 1996, p. 163.
47. A.M. Alfantazi, G. Brehaut and U. Erb, *Surf. Coat. Tech.*, 89 (1997) 239.
48. H. Natter and R. Hempelmann, *J. Phys. Chem.*, 100 (1996) 19525.